Vertical structure of surface gravity waves propagating over a sloping seabed: Theory and field measurements

Qingping Zou, Alex E. Hay, and Anthony J. Bowen
Department of Oceanography, Dalhousie University, Halifax, Nova Scotia, Canada

Received 10 April 2002; revised 2 February 2003; accepted 21 March 2003; published 16 August 2003.

[1] Theoretical predictions of the vertical structure of wave motion over a sloping seabed are compared with field observations close to the bed in the nearshore zone. Of particular interest is the effect of the local slope on the magnitude and phase of the vertical velocity. Field measurements of near-bed velocity profiles on a 2° bed slope were obtained using a coherent Doppler profiler. The surface elevation was measured by a colocated, upward looking, acoustic sounder. Results are presented from two intervals of different wave energy levels during a storm event: for wave height/water depth ratios smaller than 0.3 and for Ursell numbers smaller than 0.6. The local comparisons of magnitude and phase between the vertical velocity and surface elevation measurements are in good agreement with linear theory for a sloping bed, but differ greatly from that for a horizontal bottom, especially in the lower water column. The sloping bottom, however, has little effect on the horizontal velocity. Linear theory appears to adequately describe the transfer function between the surface elevation and the near-bed velocities, not only at the peak frequencies but also at their harmonics. However, in relatively shallow water the local transformations of free and forced waves at the harmonic frequencies are indistinguishable in the lower water column. Therefore, given surface elevation measurements at a particular location (which reflect the integrated effects of nonlinearities associated with wave shoaling), the vertical structure of the third moments of velocity fields estimated from linear theory is in reasonable agreement with the observations. Both theory and observations show that the skewness and asymmetry of the vertical velocity are subject to significant bottom slope effects, whereas those of horizontal velocity are not. *INDEX TERMS:* 4211 Oceanography: General: Benthic boundary layers; 4203 Oceanography: General: Analytical modeling; 4219 Oceanography: General: Continental shelf processes; 4546 Oceanography: Physical: Nearshore processes; 4560 Oceanography: Physical: Surface waves and tides (1255); *KEYWORDS:* shoaling waves, bottom slope, vertical structure, skewness, asymmetry, boundary layers

Citation: Zou, Q., A. E. Hay, and A. J. Bowen, Vertical structure of surface gravity waves propagating over a sloping seabed: Theory and field measurements, *J. Geophys. Res.*, *108*(C8), 3265, doi:10.1029/2002JC001432, 2003.

1. Introduction

[2] Previous studies of the effects of bottom slope on surface gravity waves in nearshore and continental shelf regions have mainly focused on the evolution of wave properties due to shoaling and refraction associated with the changes in depth on relatively large scales [*Freilich and Guza*, 1984; *Elgar and Guza*, 1985; *Liu et al.*, 1985]. While the relation between the surface displacement and the orbital velocities has been investigated, this has usually involved only a few current meters at any station (often only one), deployed well away from the seabed, measuring the horizontal velocity components. Field measurements of the vertical velocity components have been rather rare [*Elgar et al.*, 2001].

[3] The theoretical effect of the local bottom slope on the wave motion has been examined by *Chu and Mei* [1970], who carried out a WKB analysis of Stokes waves incident on a beach and found that the wave phase is affected by the rate of depth variation, and the change depends on the vertical coordinate. However, the change in the horizontal component of the velocity is small, essentially unobservable in the field because of other perturbations associated with directional spreading and the bottom boundary layer. Measurements of the vertical velocity field are therefore essential.

[4] In practice, reliable profile measurements of both the horizontal and vertical components of the wave velocity field are needed, and these measurements can now be made in the field using acoustic Doppler techniques [*Zedel and Hay*, 1999, 2002]. In this paper we compare field measurements made at Queensland Beach, Nova Scotia with theoretical predictions of the vertical structure of wave velocities and their statistical properties. The focus is primarily on the structure just above the seabed, where the effects of both the slope and the bottom boundary layer are most pronounced. One obvious point of interest is that, in the presence of

0148-0227/03/2002JC001432$09.00

bottom slope, the vertical and horizontal velocities are no longer in quadrature: nonzero wave shear stresses are therefore observed.

[5] In deep water, waves tend to have small amplitudes, strong frequency dispersion and broad directional distributions. The second-order, forced wave, correction to linear wave theory is small, as is the cross-spectral energy transfer arising from the exact quartet resonance among waves at the third order [*Phillips*, 1960; *Hasselman*, 1962]. Entering the shoaling region, however, wave frequency dispersion moderates, the direction distribution narrows, and nonlinearity becomes stronger. Near-resonant interaction among waves becomes important in cross-spectral energy transfer [*Armstrong et al.*, 1962; *Bretherton*, 1964] and is at second order instead of third order [*Mei and Unluata*, 1972; *Bryant*, 1973]. Despite the enhanced nonlinearity of waves in the shoaling region, linear finite depth theory gives reasonable predictions of the evolution of the second moments of surface elevation and horizontal velocity through the region. The linear theory, however, fails to predict the evolution of the third moments of surface gravity waves [*Freilich and Guza*, 1984; *Elgar and Guza*, 1985; *Elgar et al.*, 1990], and nonlinear Boussinesq-type models must be used instead.

[6] However, at any particular location, linear theory relatively accurately predicts the complex transfer function between the surface elevation and the wave velocity at a specific height in the shoaling region [*Guza and Thornton*, 1980; *Herbers et al.*, 1992; *Drennen et al.*, 1992]. In the surf zone, for large values of the ratio of wave height to water depth, H/h, some departures from a linear transformation become observable at the harmonic frequencies, particularly at the third harmonic [*Elgar et al.*, 2001]. The coherent Doppler profiler systems used in this study acquire surface elevations and velocity profiles synoptically. We can therefore examine whether the predictions of linear theory, based on the surface elevation measurements, accurately describe the observed vertical structure of the velocity field. For the irregular waves typical of field conditions, we are also interested in whether linear theory can predict the vertical structure of the higher-order wave velocity statistics, such as the variance, skewness and asymmetry.

[7] *Zou and Hay* [2003] obtained the analytical solutions for wave velocity and shear stress within wave bottom boundary layer (WBL) over a sloping bottom. The predicted velocities and shear stress were in reasonably good agreement with the field observations. Both theoretical predictions and field observations indicated a significant sloping bottom effect on the vertical velocity profile within the WBL.

[8] In this paper, we use the observed surface elevations and the combination of *Chu and Mei*'s [1970] potential flow theory with the WBL theory by *Zou and Hay* [2003] to obtain wave orbital velocity predictions for the entire water column. The objective is to examine the effects of the sloping bottom on the vertical structure of the magnitudes and phases of the orbital velocity components, and on their second and third moments. We present our work in the following order. First, the matched velocity solutions are obtained in section 2. In section 3, we briefly describe the field instrumentation, observations and data analysis. The field measurements are then compared with the theory in section 4. The implications of these comparisons are discussed further in section 5. Finally in section 6, we conclude by summarizing the major findings of this study.

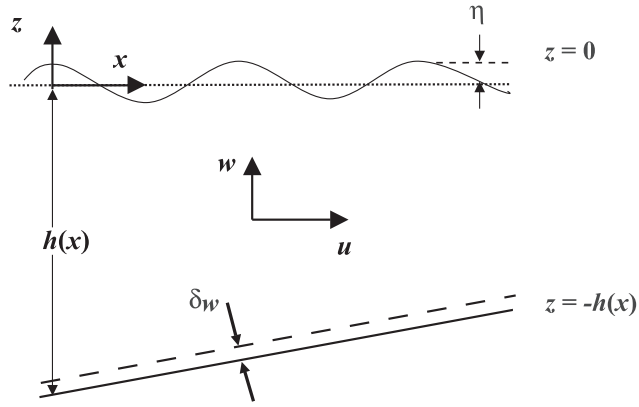

Figure 1. Definition sketch of variables and coordinate system for waves propagating over a planar, sloping seabed.

2. Theory

[9] We consider here the vertical transformation of velocity beneath shoaling waves propagating over a sloping seabed with a spatial scale of many wavelengths, i.e., $|\vec{\nabla}_H h|/(kh) = O(ka) \equiv O(\varepsilon)$ where $\vec{\nabla}_H$ is the horizontal gradient operator, h is the water depth, k is the wave number, and a is the surface elevation amplitude. First, we derive the wave velocities for the interior region from *Chu and Mei*'s [1970] velocity potential solutions for Stokes waves in variable water depth. Then by matching these solutions with those for the WBL by *Zou and Hay* [2003], we obtain solutions valid through the full water column and which satisfy the no-slip boundary condition at the bed. As by *Zou and Hay* [2003], the thickness of WBL is taken as $\delta_w = \kappa u_*/\omega$, where $\kappa \approx 0.4$ is von Karman's constant, u_* is the friction velocity and ω is the wave radian frequency.

2.1. Interior Region ($z + h \gg O(\delta_w)$)

[10] Following ***Chu and Mei*** [1970], the horizontal coordinate x is positive toward shore, and the vertical coordinate z is positive upward, with $z = 0$ at the mean free surface and $z = -h(x)$ at the bottom (see Figure 1). The basic wave equations for unsteady, incompressible, irrotational and inviscid flow are [cf. *Mei*, 1989, chaps. 1 and 12],

$$\nabla^2\Phi = \nabla_H{}^2\Phi + \Phi_{zz} = 0 \quad -h(x) \le z \le \eta(x,t), \tag{1}$$

$$\Phi_{tt} + g\Phi_z + \left(\frac{\partial}{\partial t} + \frac{1}{2}\vec{U}\cdot\nabla\right)|\vec{U}|^2 = 0 \quad z = \eta(x,t), \tag{2}$$

$$\Phi_z + \vec{\nabla}_H\Phi\cdot\vec{\nabla}_H h = 0 \qquad z = -h(x), \tag{3}$$

where Φ is the velocity potential,

$$\vec{U} = \vec{\nabla}\Phi \tag{4}$$

is the velocity vector, the free surface elevation is related to the potential by

$$\eta = -\frac{1}{g}\left(\Phi_t + \frac{1}{2}\left|\vec{U}\right|^2\right), \qquad z = \eta(x,t) \tag{5}$$

and the fluid density ρ has been set equal to unity.

[11] We assume the following WKB expansions for the velocity potential and surface elevation:

$$\Phi(x,z,t) = \sum_{n=1}^{\infty}\varepsilon^n \sum_{m=-n}^{n}\phi^{(n,m)}(X,Z,T)e^{im\psi}, \tag{6}$$

$$\eta(x,z,t) = \sum_{n=1}^{\infty}\varepsilon^n \sum_{m=-n}^{n}\eta^{(n,m)}(X,Z,T)e^{im\psi}, \tag{7}$$

where $X = \varepsilon x$ is the slowly varying horizontal coordinate, $T = \varepsilon t$ the slowly varying time, $Z = z$,

$$\psi = \int [k(X,T)dx - \omega(X,T)dt] \tag{8}$$

is the phase function, and

$$k = \sum_{j=1}^{\infty}\varepsilon^{2j}k_j, \tag{9}$$

$$\omega = \sum_{j=1}^{\infty}\varepsilon^{2j}\omega_j. \tag{10}$$

Assuming that the surface elevation is small, the free surface boundary conditions (2) and (5) can be expanded about $z = 0$. Substituting the WKB expansions (6) and (7) into the resulting boundary condition equations as well as into equations (1) and (3), at $O(\varepsilon^n)$ we obtain the following boundary value problem for the mth harmonic:

$$\phi_{zz}^{(n,m)} - m^2k^2\phi^{(n,m)} = R^{(n,m)}(X,Z,T), \qquad -h(x) \le Z \le 0, \tag{11}$$

$$g\phi_z^{(n,m)} - m^2\omega^2\phi^{(n,m)} = G^{(n,m)}(X,Z,T), \qquad Z = 0, \tag{12}$$

$$\phi_z^{(n,m)} = F^{(n,m)}(X,T), \qquad Z = -h(x), \tag{13}$$

and

$$\eta^{(n,m)} = \frac{1}{g}\left[im\omega\phi^{(n,m)}(X,0,T) - H^{(n,m)}(X,T)\right], \qquad Z = 0. \tag{14}$$

[12] For, $m \le 2$, $R^{(n,m)}$, $G^{(n,m)}$, $F^{(n,m)}$, and $H^{(n,m)}$, are given by *Chu and Mei* [1970] and listed in Appendix A for the reader's convenience. Also listed therein are the solutions $\phi^{(n,m)}$ and $\eta^{(n,m)}$ to equations (11)–(14) for waves incident on a 2-D bottom topography at an arbitrary angle. For simplicity, in the remainder of this paper we consider solutions for the cases of normal incident wave over 1-D bottom topography, $h = h(x)$. Substituting equations (A3a), (A3b), (A9), and (A10) into equations (4) and (6) gives the velocity solutions in the same WKB expansion form as equation (6), which may be rewritten as a sum of harmonics:

$$[U(x,t),\ W(x,t),\ \eta(t)] = \left[\sum_{n=1}^{\infty}\left(U^{(m)}, W^{(m)}, \eta^{(m)}\right)\cdot e^{im\psi} + c.c\right], \tag{15}$$

where $c.c$ denotes the complex conjugate of the preceding variable and will be omitted hereafter, ($U^{(m)}$, $W^{(m)}$, $\eta^{(m)}$) are the complex amplitudes of the mth harmonic of [$U(x, t)$, $W(x, t)$, $\eta(t)$]. The complex amplitudes of the primary wave, ($U^{(1)}$, $W^{(1)}$, $\eta^{(1)}$), are given to $O(\varepsilon^2)$ by

$$U^{(1)} = \frac{gak}{2\omega\cosh q}[1 + i(\delta + \delta_u)]\cosh Q, \tag{16}$$

$$W^{(1)} = \frac{-igak}{2\omega\cosh q}\left[(1 + i\delta)\sinh Q + i\delta_Q\cosh Q\right], \tag{17}$$

$$\eta^{(1)} = \frac{1}{2}a, \tag{18}$$

where $Q = k(z + h)$, $q = kh$,

$$\delta = -[\alpha_1(Q - q) + \alpha_2(Q\tanh Q - q\tanh q) + \alpha_3\left(Q^2 - q^2\right)], \tag{19}$$

$$\delta_u = -[\alpha_2 + 2\alpha_3 Q\tanh Q + \alpha_1\tanh Q], \tag{20}$$

$$\delta_Q = -\left[\alpha_1 + \alpha_2\left(\tanh Q + Q\,sech^2 Q\right) + 2\alpha_3 Q\right], \tag{21}$$

$\alpha_1 = h_x$, $\alpha_2 = \left(\frac{ka}{\cosh q}\right)^{-1}\left(\frac{a}{\cosh q}\right)_x$, and $\alpha_3 = \frac{k_x}{2k^2}\cdot\alpha_2$ and α_3 may be rewritten as

$$\alpha_2 = -\frac{h_x}{(1+G)^2\tanh q} \tag{22}$$

$$\alpha_3 = -\frac{1}{2q}\frac{G}{1+G}h_x. \tag{23}$$

where $G = 2q/\sinh(2q)$. The α_1, α_2, and α_3 are therefore linearly dependent on the bottom slope, h_x, and are associated with the variations of bottom elevation, wave amplitude and wave number respectively. As shown by equations (16) and (17), each velocity component is the corresponding horizontal bottom solution with added terms representing the sloping bottom perturbation. These perturbation terms are given by δ, δ_Q and δ_u which in turn are

proportional to the bottom slope, as indicated by equations (19)–(23).

2.2. Wave Bottom Boundary Layer ($z + h \sim O(\delta_w)$)

[13] The complex amplitudes of the primary wave velocities within a wave turbulent boundary layer over a sloping bed are derived by *Zou and Hay* [2003]

$$u^{(1)}_{wbl} = u^{(1)}_b \left[1 - \frac{F_1(\alpha,\zeta)}{F_1(\alpha,\zeta_0)}\right], \tag{24}$$

$$w^{(1)}_{wbl} = u^{(1)}_b \left\{ ik\omega^{-1}\left(1 - \frac{u^{(1)}_{bx}}{iku^{(1)}_b}\right)\left[\kappa u_*\zeta - i\left(\tau^{(1)} - \tau^{(1)}\big|_{\zeta=\zeta_0}\right)\right] - h_x\left[1 - \frac{F_1(\alpha,\zeta)}{F_1(\alpha,\zeta_0)}\right]\right\}, \tag{25}$$

where

$$\tau^{(1)} = \kappa u^{(1)}_b (F_1(\alpha,\zeta_0))^{-1}(1+i\alpha\zeta)^{-\frac{1}{2}}\sqrt{i\zeta}\ \frac{\mathrm{ker}_1 2\sqrt{\zeta} + i\mathrm{kei}_1 2\sqrt{\zeta}}{\mathrm{ker}2\sqrt{\zeta_0} + i\mathrm{kei}2\sqrt{\zeta_0}} \tag{26}$$

is the complex shear stress amplitude,

$$F_1(\alpha,\zeta) = (1+i\alpha\zeta)^{-\frac{1}{2}}\left[\frac{\mathrm{ker}2\sqrt{\zeta} + i\mathrm{kei}2\sqrt{\zeta}}{\mathrm{ker}2\sqrt{\zeta_0} + i\mathrm{kei}2\sqrt{\zeta_0}} + \frac{\alpha}{2}\sqrt{i\zeta}\cdot\frac{\mathrm{ker}_1 2\sqrt{\zeta} + i\mathrm{kei}_1 2\sqrt{\zeta}}{\mathrm{ker}2\sqrt{\zeta_0} + i\mathrm{kei}2\sqrt{\zeta_0}}(1+i\alpha\zeta)^{-1}\right], \tag{27}$$

(ker, kei) and (ker_1, kei_1) are the zeroth- and first-order Kelvin functions, $u^{(1)}_b = U^{(1)}\big|_{z=0}$ is the complex wave orbital velocity amplitude just outside the WBL, $\zeta = (z+h)/\delta_w$ is the stretched vertical coordinate, $\zeta_0 = z_0/\delta_w$, and $\alpha = 2$ is the turbulent relaxation coefficient in the viscoelastic diffusion model [cf. *Zou*, 2002].

2.3. Full Water Column ($-h \le z \le 0$)

[14] Assuming a relatively thin wave boundary layer, i.e., $\delta_w \ll h$, we have $U^{(1)}(z+h=z_b) \approx U^{(1)}(z+h=0)$, z_b where is a height corresponding to several boundary layer thicknesses. The following solutions are then valid for both the interior region and the wave boundary layer,

$$u^{(1)} = U^{(1)}(z)\left[1 - \frac{F_1(\alpha, z/l)}{F_1(\alpha, z_0/l)}\right], \quad \text{for } -h \le z \le 0 \tag{28}$$

$$w^{(1)} = \begin{cases} w^{(1)}_{wbl}, & \text{for } -h \le z \le -h + z_b \\ W^{(1)}(z) - W^{(1)}(z=-h+z_b) + w^{(1)}_{wbl}(z=-h+z_b), & \\ \text{for } -h + z_b \le z \le 0 & \end{cases} \tag{29}$$

[15] The transfer functions between velocity and surface elevation are then given by

$$H_{u\eta}(\omega,z) = \frac{u^{(1)}(\omega,z)}{\eta^{(1)}(\omega)}, \tag{30}$$

$$H_{w\eta}(\omega,z) = \frac{w^{(1)}(\omega,z)}{\eta^{(1)}(\omega)}. \tag{31}$$

Figure 2 demonstrates how bottom slope affects the u and w profiles over the entire water column. Predictions both with and without bottom friction are shown in the figure. The solutions show significant sloping bottom effects on both the magnitude and the phase of the vertical velocity, and a comparatively smaller effect on the phase of the horizontal velocity. From equation (16), in the interior region, the phase of $H_{u\eta}(\omega, z)$ is $\theta_{u\eta}(\omega, z) \approx \delta + \delta_u = O(h_x)$ (see equations (19)–(23)), and the magnitude of the transfer function $\left|H_{u\eta}(\omega,z)\right| = (gk/\omega \cosh q)\cosh Q + O(h_x{}^2)$. Thus the effects of the bottom slope on the magnitude of the horizontal velocity are negligible, but there is a change of the order of the bottom slope to the phase of the horizontal velocity as shown by Figure 2. Since u and w are not in quadrature, a nonzero wave shear stress $\langle uw\rangle$ is induced which, for nondissipative waves in shallow water, increases from a value of $-h_x\langle u^2\rangle/4$ at the surface to $-h_x\langle u^2\rangle$ at the bed [*De Vriend and Kitou*, 1990; *Rivero and Arcilla*, 1995]. The deviation of the phase between w and u at the surface from the 90° value for a horizontal bed is then given by $\sin\theta_{wu} = (\omega^2 h/g)^{-1/2}h_x/4$ where $\omega^2 h/g \ll 1$ so that θ_{wu} is again of the order of the bottom slope. We note that the sloping bottom effect on both the magnitude and phase of the vertical velocity decreases with increasing height above the bed, increases with slope, and decreases with frequency for a given water depth [cf. *Zou and Hay*, 2001]. Also evident in Figure 2, for w, is that while the change in phase due to the sloping bottom extends over all depths, the changes in magnitude are confined to the lower water column (cf. section 5 for more discussions).

3. Field Measurements and Data Analysis

[16] The field measurements were carried out at Queensland Beach, Nova Scotia, an O(100 m)-long, unbarred, pocket beach. The measurements were collected at a location approximately 60 m from the shoreline, in a mean water depth of 3.7 m, with a local bed slope of about 2°. Vertical and horizontal velocity profiles with 0.7 cm vertical resolution were acquired at 15-min intervals for about 8 min with a bistatic Coherent Doppler Profiler (CDP) [*Zedel and Hay*, 1999] at a profile acquisition rate of about 30 Hz, using 9 pulse pair averaging. Surface elevation was measured at 30-min intervals for about 8 min with an upward looking, pencil beam acoustic sounder at a sampling rate of 8 Hz. Bedform geometry was detected at 30-min intervals by centimeter resolution rotary side scan and pencil beam sonars, and continuously except during daylight with a millimeter resolution laser video system [*Crawford and Hay*, 1999]. More detailed descriptions of the field site and instrumentation are given by *Crawford and Hay* [2001] and *Smyth et al.* [2002].

[17] Results are presented from two intervals during a storm event when the bed state changed from flat bed at the peak of the storm to linear transition ripples with 3 mm height, 8 cm wavelength immediately afterward [*Crawford and Hay*, 2001; *Smyth et al.*, 2002]. As shown in Figures 6 and 7, the wave spectrum was somewhat bimodal during the flat bed interval, and less so during the rippled bed interval (see *Zou and Hay* [2003, Figure 3] for the spectra evolution during these intervals). Table 1 lists the wave peak frequency, wave number, water depth, significant wave height, Ursell

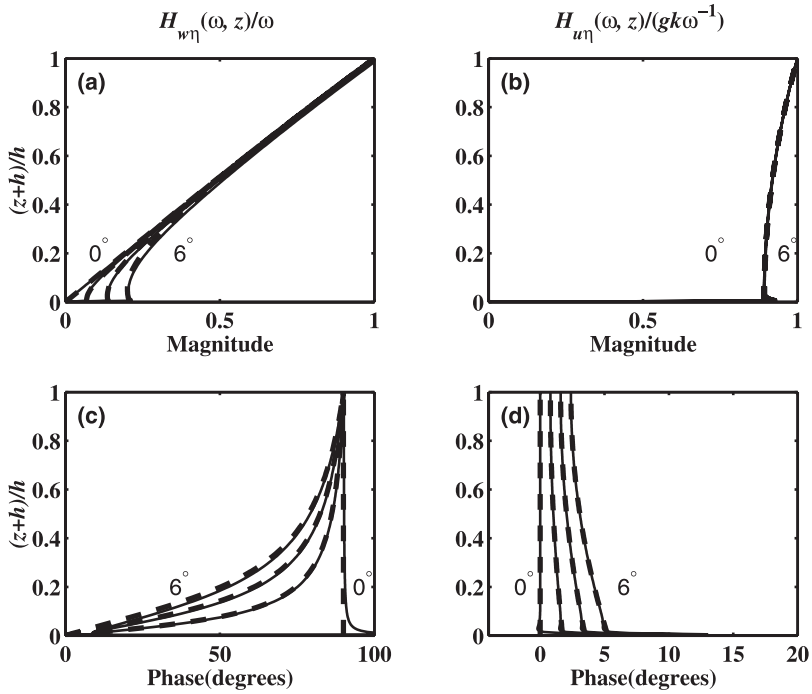

Figure 2. Vertical profiles of the magnitude and phase of the normalized transfer functions $H_{w\eta}/\omega$ and $H_{u\eta}/(gk\omega^{-1})$ and between velocity components u or w and surface elevation η: the predicted profiles at frequency $f = 0.12$ Hz according to the present theory (solid lines) for a water depth $h = 3.67$ m, bottom roughness length $r = 1.08$ cm, and friction velocity $u_* = 4.9$ cm/s and *Chu and Mei* [1970] theory (dashed lines) over bed slopes of 0°, 2°, 4°, and 6°.

number $U_r = 0.5k_pH_s/(k_ph)^3$ and ratio of significant wave height to water depth for the two intervals.

[18] Vertical profiles of near-bed velocity were measured with the CDP extending through the WBL to the bed, with 0.7 cm vertical resolution. The CDP transceivers were mounted on a cantilevered frame at a nominal height of 80 cm above bottom. The vertical velocity profiles extended to a height of about 50 cm from the bed; the horizontal velocity profiles to about 30 cm height. The velocity measurements are based on the rate of change of the phase of the scattered sound between successive pulse pairs. For this experiment, the phase change was averaged over 9 pulse pair ensembles, for which the accuracy of the vertical and horizontal velocities is expected to be about 0.17 cm s^{-1} and 0.7 cm s^{-1} respectively [*Zedel and Hay*, 2002].

[19] Because the sampling rates for the upward looking pencil beam sonar and the CDP were different, the surface elevation measurements were interpolated to the CDP profile time base. Power spectra S_{uu}, S_{ww}, and $S_{\eta\eta}$ of the velocity components (u, w) and surface elevation η, and cross-spectra $C_{u\eta}$ and $C_{w\eta}$, were computed using Welch's averaged periodogram method and a Hanning window, dividing each 8-min data run into demeaned and detrended 2048-sample segments overlapped by 75%. Degrees of freedom n_d are 70 and 82 for the average spectra for the flat and rippled bed intervals respectively.

[20] Transfer functions were obtained from the autospectra and cross-spectra according to

$$H_{u\eta}(\omega, z) = \frac{C_{u\eta}(\omega, z)}{S_{\eta\eta}(\omega)} \tag{32}$$

$$H_{w\eta}(\omega, z) = \frac{C_{w\eta}(\omega, z)}{S_{\eta\eta}(\omega)} \tag{33}$$

The magnitudes of the transfer functions may rewritten as

$$\left|H_{u\eta}(\omega, z)\right| = \left[\gamma^2_{u\eta}(\omega, z)\frac{S_{uu}(\omega, z)}{S_{\eta\eta}(\omega)}\right]^{\frac{1}{2}} \tag{34}$$

$$\left|H_{w\eta}(\omega, z)\right| = \left[\gamma^2_{w\eta}(\omega, z)\frac{S_{ww}(\omega, z)}{S_{\eta\eta}(\omega)}\right]^{\frac{1}{2}} \tag{35}$$

where $\gamma^2_{u\eta}(\omega, z) = \frac{\left|C_{u\eta}(\omega,z)\right|^2}{S_{uu}(\omega,z)S_{\eta\eta}(\omega)}$ and $\gamma^2_{w\eta}(\omega, z) = \frac{\left|C_{w\eta}(\omega,z)\right|^2}{S_{ww}(\omega,z)S_{\eta\eta}(\omega)}$ are the corresponding coherence functions. The magnitude of the transfer function is equal to the ratio between spectra multiplied by the square root of the coherence function; therefore, in case of low coherence the former can be substantially smaller than the latter. This result is observed in the comparisons of spectra and transfer functions in the next section. Confidence intervals (95%) for the transfer

Table 1. Wave Peak Frequency f_p, Wave Number k_p, Water Depth h, Significant Wave Height H_s, Ursell Number $U_r = 0.5k_pH_s/(k_ph)^3$, and Ratio of Significant Wave Height to Water Depth H_s/h for Flat and Rippled Bed Intervals

Intervals	f_p, Hz	k_p, m^{-1}	h, m	H_s, m	U_r	H_s/h
Flat bed	0.12	0.13	3.7	1.1	0.64	0.30
Rippled bed	0.12	0.15	3.1	0.74	0.55	0.24

functions were estimated using the relationship [*Bendat and Piersol*, 1986, section 9.2.4]:

$$\overline{|H|}(1-2\Delta) \le |H| \le \overline{|H|}(1+2\Delta), \tag{36}$$

where $|\bar{H}|$ and |H| are the estimated and expected values for the magnitude of the transfer functions, the subscripts (u, η) and (w, η) are omitted, and Δ is the normalized random error

$$\Delta = \frac{[1-\gamma^2(\omega)]^{\frac{1}{2}}}{|\gamma(\omega)|\sqrt{2n_d}}, \tag{37}$$

where γ^2 (ω) is the corresponding estimated coherence. According to *Bendat and Piersol* [1986], the standard deviation of the transfer function phase measured in radians is approximately equal to the normalized random error of the transfer function magnitude.

4. Comparisons Between Theory and Measurements

4.1. Transfer Functions Between Velocity and Surface Elevation

[21] One method we use to compare predicted and measured wave orbital velocities is based on the transfer functions (also called the frequency response function by *Bendat and Piersol* [1986]) between velocity at depth and the surface elevation. Being normalized, an advantage of the transfer function approach is that averaging can be carried out over the transfer functions for different runs with somewhat different energies: for example, the different runs in the flat bed interval. This averaging reduces the noise in the estimates of magnitude and phase at each frequency. A second reason for introducing the transfer function here is related to the broader question of the applicability of linear theory locally, i.e., the question of whether local measurements of surface elevation combined with linear wave theory can reproduce velocities observed under shoaling waves in the sea swell band . This question was raised in the Introduction, and we return to it in the discussion section.

[22] For each 8-min data run, the Fourier components of the band-pass filtered surface elevation, determined by fast Fourier transform (FFT), are multiplied by the transfer function solutions $H_{u\eta}$ (ω, z) and $H_{w\eta}$ (ω, z), equations (30) and (31) in combination with equations (28) and (29), to obtain the predicted Fourier components of velocity at a given height above bottom, $z + h$. These Fourier components are then used to reconstruct predicted ($u(z, t)$, $w(z, t)$) time series by inverse FFT. Figure 3 is an example, showing the observed surface elevation time series, and the corresponding velocities at 10 cm above the bed: the observed velocities are indicated by gray lines, the predictions by dark lines. The predicted horizontal and vertical velocities are both in good agreement with the observations.

[23] Figure 4 shows the comparison in the frequency domain between the predicted and observed transfer function magnitudes and phases at 10 and 20 cm height, for the flat bed interval. The observed values of $|H_{w\eta}|$ (denoted by plus signs) are consistent with the predictions for a sloping bottom, but differ significantly from those for a horizontal bottom (Figures 4a and 4b). The predicted values of $|H_{w\eta}|$

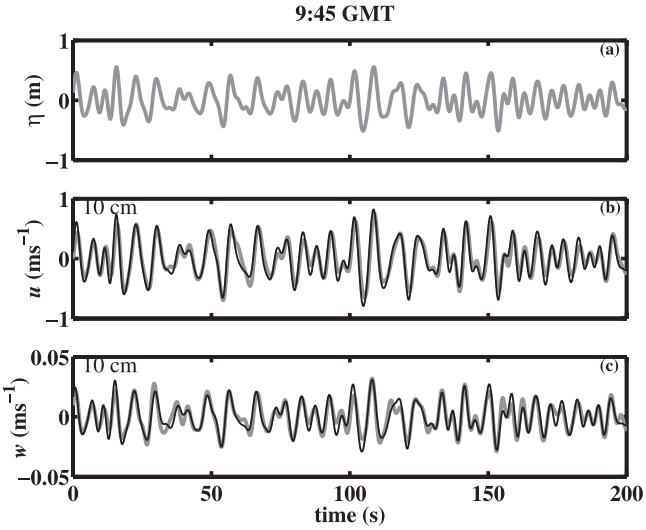

Figure 3. (a) Surface elevation η, (b) horizontal velocity u, and (c) vertical velocity w (velocities at 10 cm above the bed) for the 200 s data run starting at 9:45 GMT on yearday 261, 1995, during flat bed interval. Gray lines are observations, and dark lines represent the predicted u and w by the present sloping bottom theory based on the observed surface elevation η.

for a sloping bottom attain a maximum at about 0.25 Hz at 20 cm height. This maximum is also indicated by the observations at 20 cm height, but disappears from both the observations and the sloping bed predictions at 10 cm. This indicates the increasing influence of bottom boundary condition on w as the bed is approached, since a similar maximum is neither predicted nor observed for $|H_{u\eta}|$ (Figures 4e and 4f). It is also evident from Figures 4a and 4b that the differences between the predictions for $|H_{w\eta}|$ with and without bottom slope increase with decreasing frequency as well as with decreasing height above bed.

[24] The observed phases of $H_{w\eta}$ are also consistent with the predictions for a sloping bottom (see Figures 4c and 4d), and as with the magnitudes, differences between the predicted phase with and without bottom slope are larger for lower frequencies and smaller heights. When there is no bottom slope, the predicted phase of $H_{w\eta}$ remains almost constant at 90° regardless of frequency, whereas with a bottom slope of 2°, the phase increases from about 10° to about 90° at both heights as frequency increases from 0.05 Hz to 0.4 Hz, consistent with the observations.

[25] As shown in Figures 4e and 4f, the predicted and observed magnitudes of the horizontal velocity transfer function are in reasonable agreement, and the predictions are changed very little by a 2° bottom slope. The predicted phases of $H_{u\eta}$ for a sloping bottom (solid lines) are only about 2° larger than those for a horizontal bottom (dash-dotted lines) and , unlike the phase of $H_{w\eta}$, remain almost independent of frequency at both heights. The observed phases of $H_{u\eta}$ are somewhat noisy (not surprising given the small values involved), but are generally consistent with the sloping bottom predictions. Note that the results in Figure 4 indicate that the phase difference between the horizontal and vertical velocity at a given height above the bed is frequency-dependent.

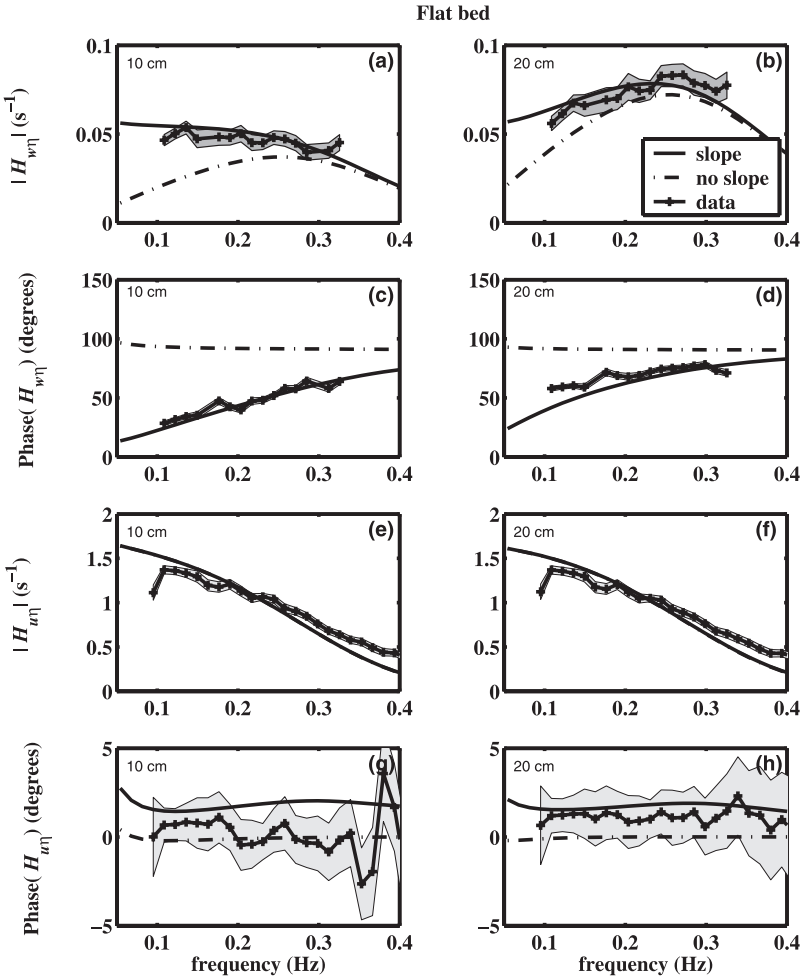

Figure 4. The predicted and observed magnitude and phase of the transfer functions versus frequency, (a)–(d) $H_{w\eta}$ and (e)–(h) $H_{u\eta}$ at 10 cm and 20 cm above the bed for the flat bed interval: the predictions for a bed slope of 0° (dash-dotted lines), 2° (solid lines), the observations (plus signs). Only the observations with coherence between velocities and surface elevation larger than 0.5 are shown. The gray shading represents the 95% confidence interval.

[26] The predicted and observed profiles of the magnitude and phase of $H_{w\eta}$ and $H_{u\eta}$ at the wave peak frequency are compared in Figure 5, for the flat bed interval. The observed magnitude and phase profiles for $H_{w\eta}$ are in good agreement with the sloping bed theory, especially in the near-bed region where the horizontal bottom predictions are incorrect. The sloping bottom effects on the magnitude of $H_{u\eta}$ are again negligible, and again a small phase shift in $H_{u\eta}$ is predicted, which is roughly the same at all depths. The observed $H_{u\eta}$ magnitudes are somewhat smaller than those predicted: this difference is likely due to that fraction of the total wave band velocity variance associated with directional spreading in the incident waves, which is not included in the observations since the v component was not measured, but is included in the predictions since they are based on the observed sea surface elevations.

[27] These same model-data comparisons were conducted for the rippled bed interval. The results are similar to those in Figures 4 and 5.

4.2. Velocity Spectra

[28] The predicted velocity spectra, S_{ww} and S_{uu}, at a given height can be obtained from the measured surface elevation spectrum $S_{\eta\eta}$ (ω) and the transfer function solutions using the following relationship,

$$S_{ww}(\omega, z) = \left|H_{w\eta}(\omega, z)\right|^2 S_{\eta\eta}(\omega) \tag{38}$$

$$S_{uu}(\omega, z) = \left|H_{u\eta}(\omega, z)\right|^2 S_{\eta\eta}(\omega) \tag{39}$$

where $|H_{w\eta}(\omega, z)|$ and $|H_{u\eta}(\omega, z)|$ are given by equations (30) and (31) in combination with equations (28) and (29). The predicted spectra are compared with the observations at heights of 10 and 20 cm above the bed in Figures 6 and 7 for the flat and rippled bed intervals respectively. The predicted vertical velocity spectra for a slope of 2° (solid lines) are in good agreement with observations (dashed lines) throughout the sea swell frequency band , 0.05–0.4 Hz.

4.3. Second- and Third-Order Velocity Moments

[29] For each 8-min data run, following the same procedure as described in section 4.1, the predicted time series of ($u(z, t)$, $w(z, t)$) at a given height above the bed were calculated from on the observed sea surface elevation time

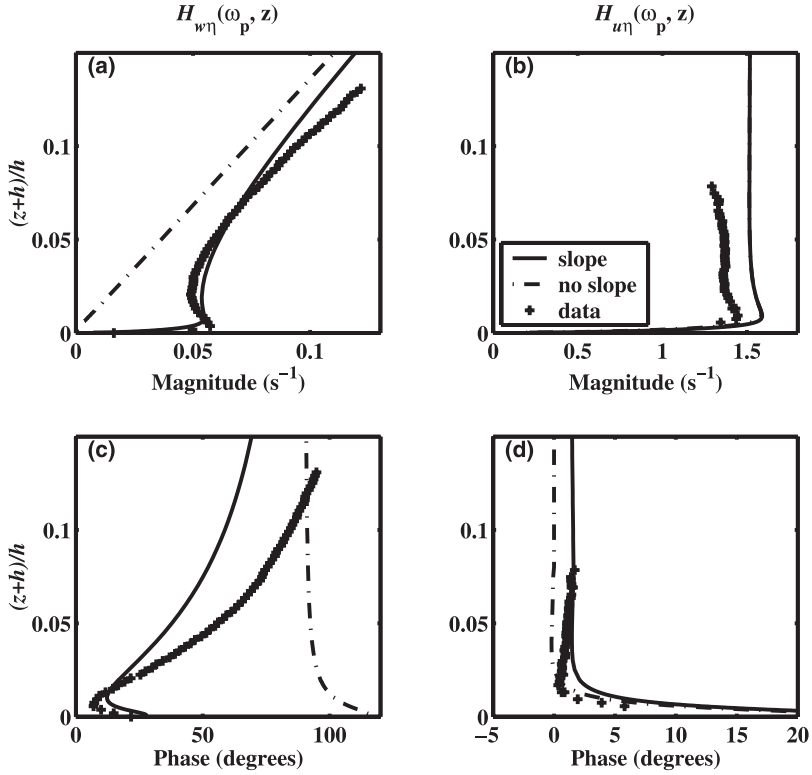

Figure 5. Vertical profiles of the magnitude and phase of the transfer functions (a) and (b) $H_{w\eta}$ and (c) and (d) $H_{u\eta}$ at the wave peak frequency for the flat bed interval: theory with bottom friction for a bed slope of 0° (dash-dotted lines) and 2° (solid lines); the observations are denoted with plus signs.

series. The second and third moments [$\langle u^2 \rangle$, $\langle w^2 \rangle$] and [$\langle u^3 \rangle$, $\langle w^3 \rangle$] were obtained from these time series, and then ensemble averaged over all data runs in each of the flat and rippled bed intervals.

[30] Vertical profiles of $u_{rms} = \langle u^2 \rangle^{\frac{1}{2}}$ and $w_{rms} = \langle w^2 \rangle^{\frac{1}{2}}$ are shown by Figure 8, and are similar to the profiles of $|H_{w\eta}(\omega_p, z)|$ and $|H_{u\eta}(\omega_p, z)|$, shown in Figure 5 and discussed in section 4.1. The predicted w_{rms} profiles, with

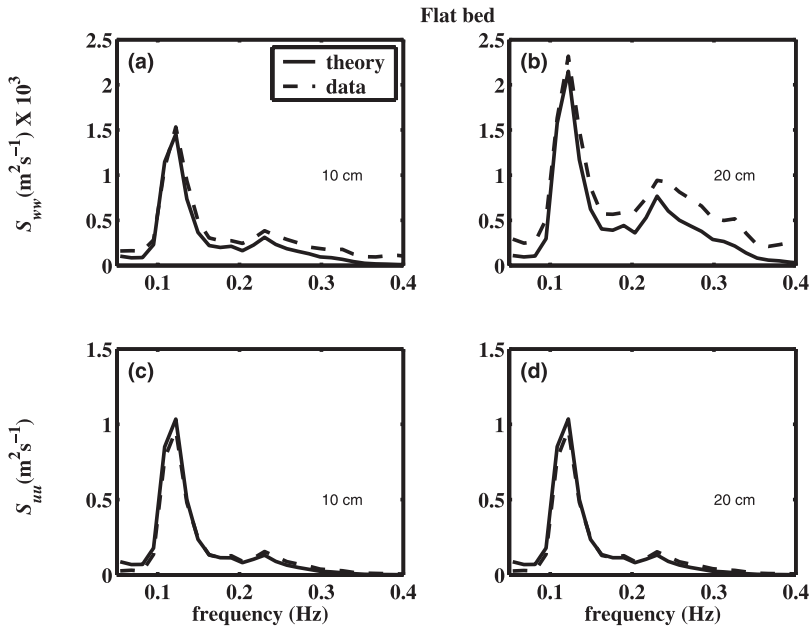

Figure 6. Velocity spectra at 10 cm and 20 cm above the bed for the flat bed interval: predicted (solid lines) and observed (dashed lines). Predictions are based on the measured surface elevation spectra and linear theory with bottom friction. (a) and (b) Vertical velocity spectra S_{ww} and (c) and (d) horizontal velocity spectra S_{uu}.

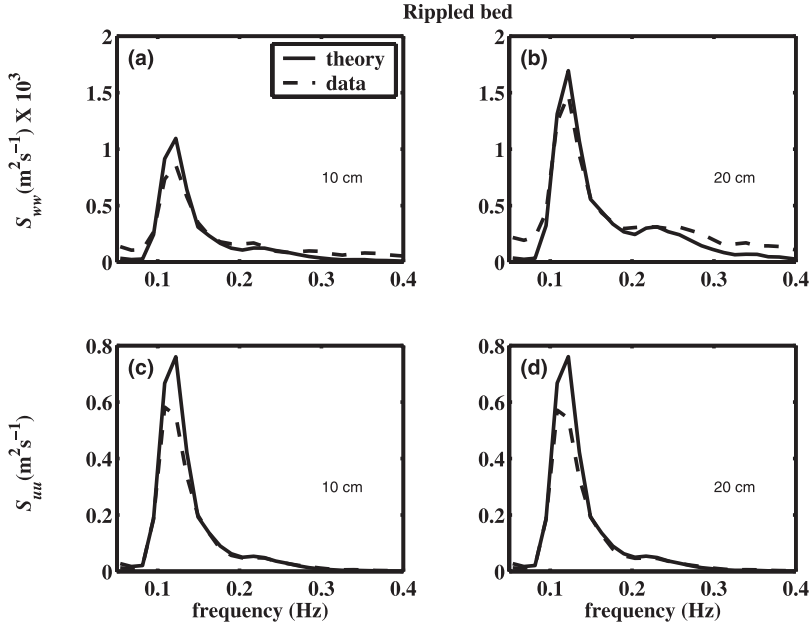

Figure 7. The predicted and observed velocity spectra at 10 cm and 20 cm above the bed. Same as Figure 6 except for the rippled bed interval.

bottom slope included (solid lines), are in good agreement with observations. The predictions without bottom slope (dash-dotted lines) underestimate the observations especially in the near-bed region (Figure 8). The observed overshooting of w_{rms} in the WBL is accurately predicted by the sloping bottom theory, but not by that for a horizontal bottom. The sloping bottom effects on u_{rms} are negligible through the water column, and the predicted values of u_{rms} are slightly larger than the observations, as expected on the basis of the results in section 4.1.

[31] The ensemble-averaged skewness is given by

$$S_u = \frac{\langle u^3 \rangle}{\langle u^2 \rangle^{3/2}} \tag{40}$$

$$S_w = \frac{\langle w^3 \rangle}{\langle w^2 \rangle^{3/2}}. \tag{41}$$

The ensemble-averaged asymmetry, A_u and A_w, are calculated in the same fashion from the Hilbert transform of u and w for both intervals.

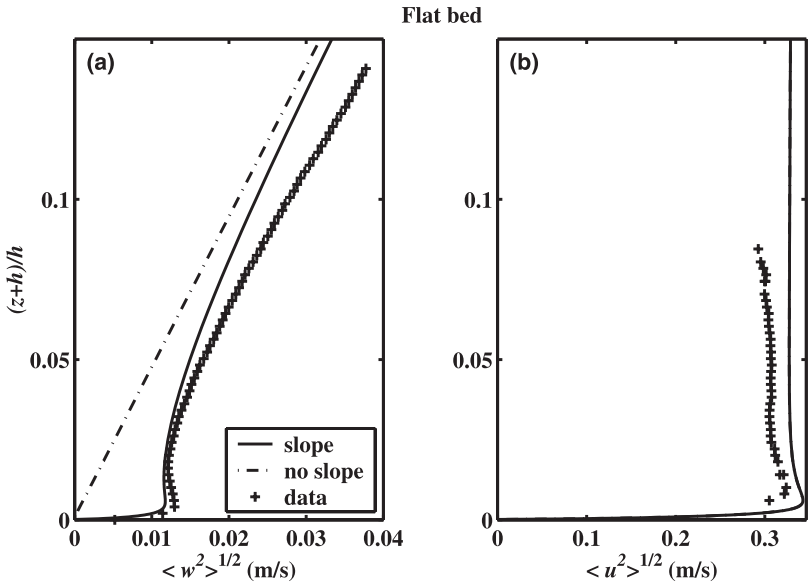

Figure 8. Vertical profiles of the root mean square of (a) w and (b) u for a frequency range of 0.08–0.3 Hz for the flat bed interval: theory with bottom friction for a bed slope of 0° (dash-dotted lines) and 2° (solid lines); the observations are denoted with plus signs.

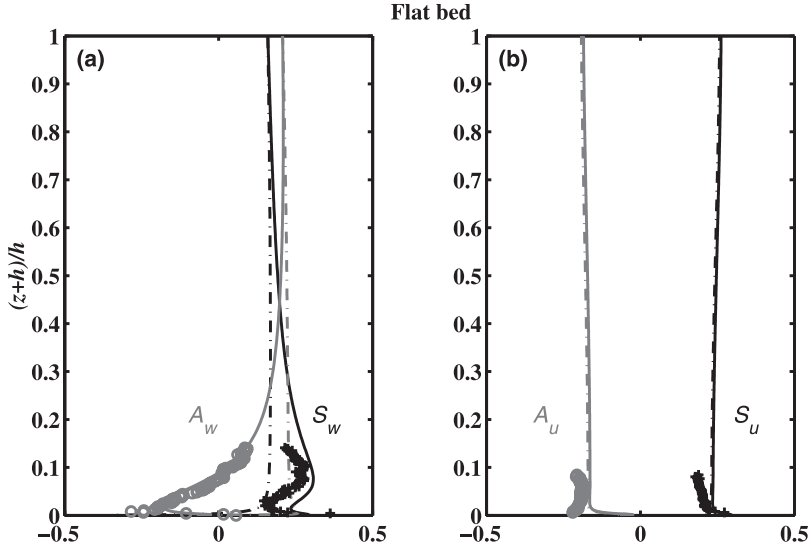

Figure 9. Predicted and observed profiles of the skewness (black) and asymmetry (gray) for (a) vertical and (b) horizontal velocity for the flat bed interval: Theory based on the surface elevation measurements with bottom friction: predictions for a bed slope of 0° (dashed lines) and 2° (solid lines); the observed skewness (+) and asymmetry (o).

[32] The predicted and observed profiles of skewness and asymmetry are compared in Figures 9 and 10 for the flat bed interval, and in Figures 11 and 12 for the rippled bed interval. Each pair of figures shows the comparisons for the full water column and in the near-bed region.

[33] In the absence of bed slope, the predicted vertical velocity skewness and asymmetry, S_w and A_w, remain constant through the full water column except for the sudden decrease within the wave bottom boundary layer. When bottom slope is included, the predicted S_w increases away from the mean free surface, attains a maximum at about one tenth of the water depth, decreases toward the top of the WBL, and then increases toward the bed. The predicted A_w decreases monotonically away from the mean free surface, changes sign, reaches a maximum negative value at the top of the WBL, and then increases toward the bed. The effects of bed slope on the skewness and asymmetry of horizontal velocity, S_u and A_u, are negligible throughout the water column. S_u and A_u decreases slightly with depth except in the WBL where both are predicted to change rapidly and to attain a local maximum.

[34] For both flat and rippled bed intervals, the predicted third moments of both velocity components compare well with the observations, especially outside the WBL, in terms of sign, profile shape and , in most instances, magnitude. The vertical velocity skewness is overpredicted in both intervals. The behavior of these moments within the WBL is not well reproduced by the theory, for either of the two velocity components. The model-data differences for the vertical velocity moments are somewhat larger for the rippled bed interval. This behavior may be due to the smaller vertical velocity amplitude at the harmonic frequency during the

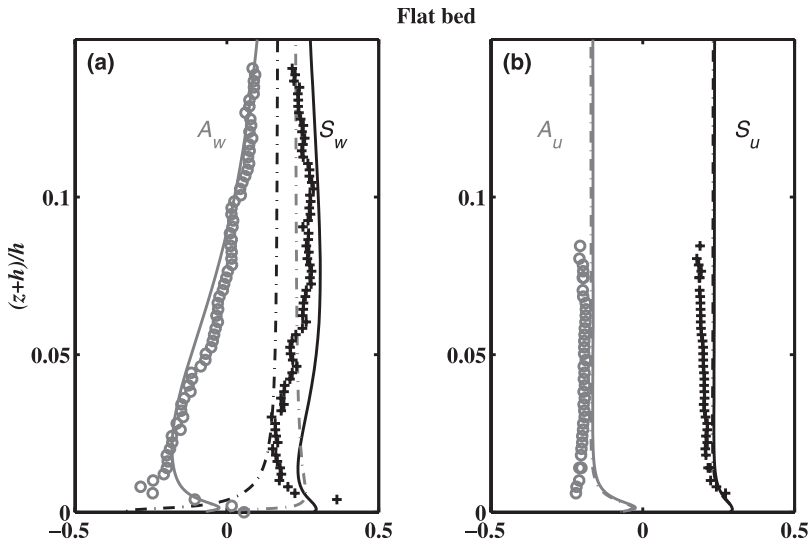

Figure 10. Same as Figure 9 except for the near-bed region.

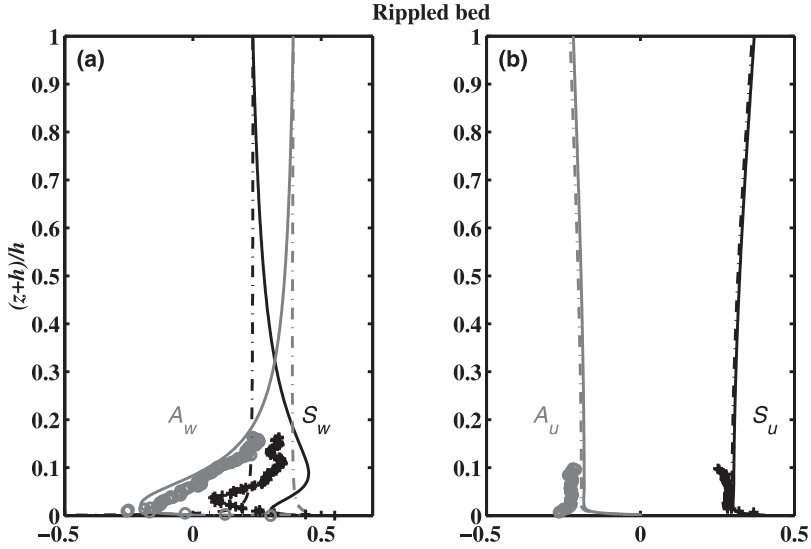

Figure 11. Predicted and observed profiles of the skewness (black) and asymmetry (gray) of (a) vertical and (b) horizontal velocities. Same as Figure 9 except for the rippled bed interval.

rippled bed interval (see Figures 6 and 7), and reduced coherence between vertical velocity and surface elevation at the harmonic frequency during this interval [cf. *Zou and Hay*, 2003].

[35] Similar comparisons for the nonnormalized third moments for the flat bed interval are presented in Figure 13. Similar to the second moment velocity profiles shown in Figure 8, the magnitudes of the nonnormalized third moments of w decrease rapidly toward the bed. The predicted nonnormalized third moments of w with bottom slope are in good agreement with the observations, whereas those without bottom slope underestimate the observations. Different from the second moments, however, the bottom slope effects on the nonnormalized third moments of w increase with height above the bed mainly because of the increasing magnitude of w. The nonnormalized asymmetry of w changes sign toward the bed. Similar to the second moments, the nonnormalized third moments of u are uniform throughout the water column except for the WBL. Further toward the bed, the third moments of u and w display an overshoot as the second moments shown in Figure 8. The predictions compare well with the observations.

[36] The predicted third moment of w with and without bottom friction for a sloping bottom are also compared with the observations (not shown here). The comparison indicates that the observed sharp changes of the third moments of velocity fields within the WBL are the results of combination effects of bottom friction and bottom slope. The same model-data comparisons were conducted for the rippled bed interval, and the results are similar to those displayed by Figure 13; therefore they are omitted in the presentation.

5. Discussion

[37] Each of the solutions (16) and (17) for the velocity field beneath waves propagating over a sloping bottom is

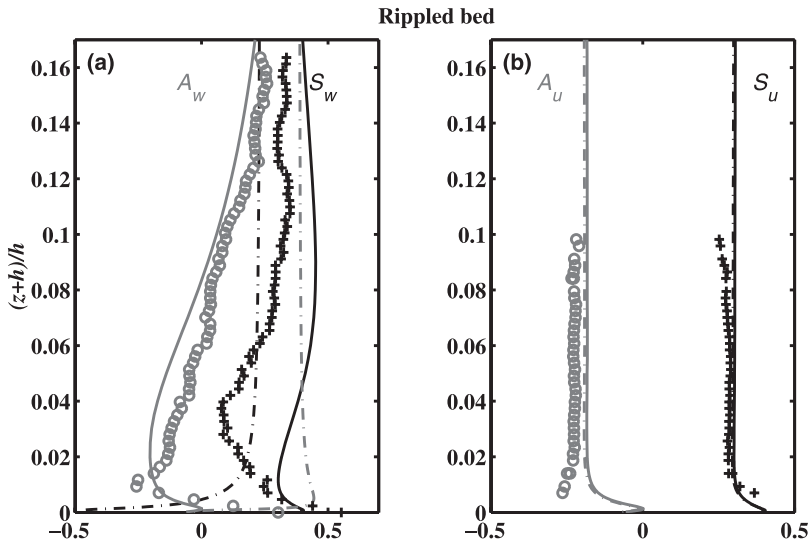

Figure 12. Same as Figure 11 except for the near-bed region.

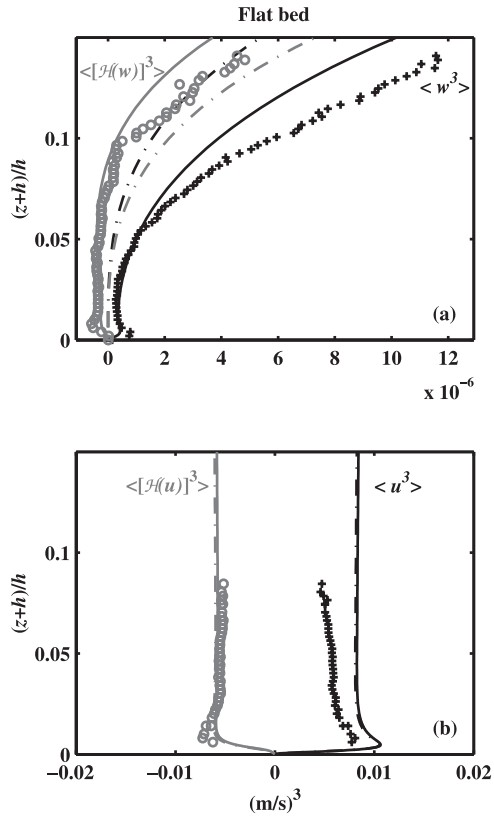

Figure 13. Predicted and observed profiles of the third moments of u and w (black) and the third moments of the Hilbert transforms H(w) and H(u) (gray) (i.e., nonnormalized skewness and asymmetry) for the flat bed intervals: (a) vertical velocity and (b) horizontal velocity.

the sum of a horizontal bottom part and a sloping bottom perturbation which are in quadrature. According to equations (16)–(23), the sloping bottom perturbations are proportional to bottom slope h_x, and are dependent on relative water depth $\omega^2 h/g$, frequency ω and altitude $z + h$ (see *Chu and Mei* [1970, Figure 2a] for δ). Both the horizontal bottom and the sloping bottom perturbation parts of the solution for the u component are proportional to cosh $k(z + h)$, while those for are proportional to sinh $k(z + h)$ and cosh $k(z + h)$ respectively. Thus, for nearly shallow water waves, the horizontal bottom part of the vertical velocity solution decreases linearly to zero at the bed, while the sloping bed perturbation part is almost uniform throughout the water column. It follows that the sloping bottom perturbation of w becomes comparable in magnitude to the horizontal bottom contribution as the bed is approached, while the perturbation of u remains small (Figure 2). In addition, the phase difference between w and u, which is close to 90° at the surface, decreases to nearly 0° at the bed in the presence of bottom slope, as required by the surface and bottom boundary conditions (Figure 2).

[38] For a significant wave height of about 1 m in a water depth of about 3.7 m (cf. Table 1), nonlinear wave-wave interactions may contribute a significant fraction of wave energy at harmonic frequencies, so that the surface elevation and velocity spectra can include contributions from both free and forced waves at these frequencies. Bispectral analysis has been applied to evaluate the contribution of forced secondary waves [*Elgar and Guza*, 1985; *Herbers et al.*, 1992]. Both the magnitude and phase of the forced wave differ from the free waves due to nonlinear effects. Nevertheless, the complex transfer functions between surface elevation and velocity are consistent with linear theory even at harmonic frequencies (Figures 4–8). As shown in Figure 14, the velocity profiles beneath free and forced waves at the first harmonic frequency $f = 2f_p$ differ only slightly near the surface, the deviation increases slightly for shorter wave period $f = 3f_p$. In the lower water column, however, the differences are negligible at both frequencies. Thus, in the local transformation from surface elevation to velocity in relatively shallow water, free and forced waves are indistinguishable in the near-bed region.

[39] *Guza and Thornton* [1980], *Herbers et al.* [1992], and *Drennan et al.* [1992] drew similar conclusions from their local comparison of point measurements of velocity under waves. These field experiments, however, were conducted in deeper water and higher in the water column where bottom effects are less important, and were therefore not detected in the measurements. *Elgar et al.* [2001] concluded, from local comparisons of velocity and surface elevation spectra in surf zone, that departures from linear theory in the local transformation increase with increasing ratio of wave height to water depth, H/h, but are negligible

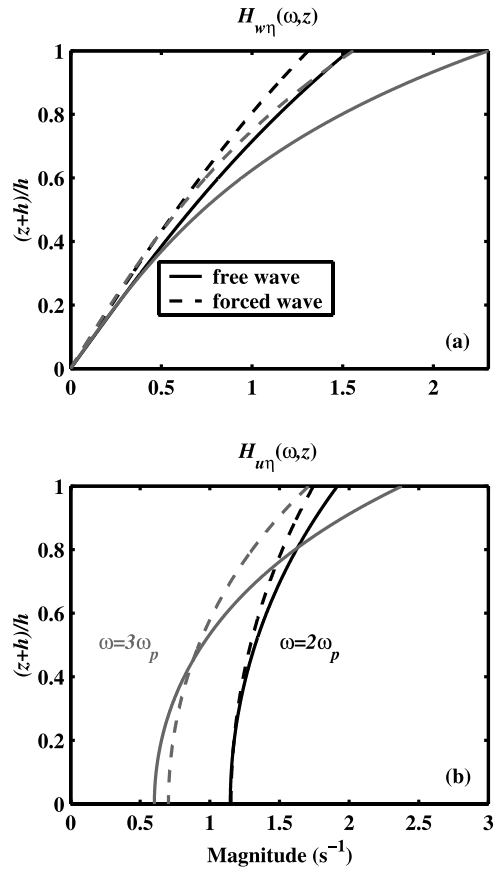

Figure 14. Vertical profiles of the magnitude of the transfer functions (a) $H_{w\eta}$ and (b) $H_{u\eta}$ for free (solid lines) and forced waves (dashed lines) at double (dark) and triple (gray) the wave peak frequency given by wave theory.

when this ratio is smaller than 0.3. For the flat and rippled bed intervals here (see Table 1), $H_s/h = 0.30$ and 0.24, and the transfer functions between surface elevation and velocity are accurately described by linear theory. This result is consistent with the findings of *Elgar et al.* [2001].

[40] Velocity skewness and asymmetry are related to the phase coupling between primary and harmonic waves. For unimodal, narrow banded wave energy spectra, skewness and asymmetry are dominated by the self-self interaction ($f_p, f_p, 2f_p$), where f_p is the wave peak frequency [*Elgar and Guza*, 1985; *Doering and Bowen*, 1987; *Elgar et al.*, 1990; *Herbers et al.*, 1992]. The phase coupling between wave components is quantitatively described by the bispectrum. As pointed out in the introduction, nonlinear Boussinesq-type models are necessary to predict the cross-shore transformation of third moments and the bispectrum through the shoaling region. However, since the local transformation of free and forced waves is indistinguishable near the bed, the third moments and bispectra of velocity are predicted reasonably accurately from the local surface elevation using linear theory.

[41] The vertical structure of the third moment of w is presented in Figures 9–12. At the surface, the vertical velocity must satisfy the same kinematic and dynamic boundary conditions (2) and (5) regardless of bottom slope, that is, $w = \eta_t$ and $\eta_x = -u_t/g$ at the leading order. Thus, at the surface and for small bottom slopes, the primary and harmonic wave components of w and u are almost in quadrature, so that $A_w \approx S_u$ and $S_w \approx -A_u$.

[42] In relatively shallow water and in the absence of bottom slope, the amplitude and phase of the first harmonic of w relative to those of the primary wave are almost constant throughout the water column, as are S_w and A_w. Therefore $A_w \approx S_u$ and $S_w \approx -A_u$ as depth increases away from the surface, except in the WBL. Furthermore, the depth attenuation of the first harmonic of u is only slightly larger than that of the primary wave, so the horizontal bottom predictions for S_u and A_u experience only a slight decrease toward the bed as shown in Figures 9 and 11.

[43] In the presence of bed slope, however, the bottom boundary condition requires that w and u be in phase near the bed, so $A_w = A_u$ and $S_w = S_u$. Thus, starting from the surface where $S_u > -A_u > 0$, the vertical velocity asymmetry A_w decreases monotonically from a positive value of S_u to a negative value of A_u at the bed outside the WBL; while the vertical velocity skewness S_w increases from a positive value of $-A_u$ to a maximum value at $z/h = 1/10$, and then decreases to a smaller positive value S_u of at the bed.

[44] In the presence of bottom slope, the harmonic and primary wave components of u and w are almost in quadrature, but are in phase at the bed. Therefore the biphase of the self-self interaction triad decreases by 90° from the surface to the bed. At the surface, with and without bottom slope, $A_w \approx S_u > 0$ and $S_w \approx -A_u > 0$, the biphase of the triad at the peak frequency is between 0° and 90°. Because of bottom slope effects, the biphase of the triad decreases by 90° to between −90° and 0° toward the bed. As a result, the real part of the bispectrum increases to a maximum and then decreases to a smaller positive value at the bed, whereas the imaginary part decreases monotonically from a positive value at the surface to a negative value toward the bed. The third moments of velocity fields beneath a unimodal wave are governed by the self-self interaction triad at the peak frequency. The skewness and asymmetry of the vertical velocity are related to the real and imaginary part of the bispectrum, and therefore display similar vertical structure (Figures 9–12).

6. Summary and Conclusions

[45] Predictions of the vertical structure of wave orbital velocities and related statistics, made using the Chu and Mei theory for surface gravity waves propagating over a sloping seabed, extended to include the turbulent wave bottom boundary layer (WBL), have been shown to compare favorably with field measurements made in the lower part of the water column. The comparisons are for moderate wave heights ($H_s/h < 0.3$) in 3.1 and 3.7 m mean water depths, a bottom slope of 2°, and for both flat and rippled bed conditions. For the data runs included in the analysis, peak wave periods for the flat and rippled bed cases were the same (about 8 s). The energy spectra, however, were distinctly bimodal for the flat bed runs, and nearly unimodal for the rippled bed runs.

[46] The sloping bottom effects on vertical velocity, evident in both magnitude and phase, are enhanced near the bed and extend well above the WBL into the interior flow. For horizontal velocity, only the phase is sensitive to bottom slope. Similarly, the vertical structure of the third-order velocity moments (i.e., skewness and asymmetry) for w are highly sensitive to bottom slope, while the vertical structure of the corresponding moments of u are not. Thus the vertical velocity profiles provide the most sensitive test of the theory.

[47] For the range of Ursell numbers and wave height/water depth ratios spanned by the present observations, linear theory is shown to adequately reproduce the complex-valued transfer function between observed local surface elevation and the vertical structure of the wave orbital velocities over the sea and swell wave frequency band. This is expected as, for relatively shallow water, the local vertical transformations of free and forced waves, predicted by the Chu and Mei theory, are indistinguishable in the lower water column and the nonlinear effects associated with wave shoaling are necessarily realized in the direct measurements of surface elevation at that specific location.

[48] Thus velocity time series at depth can be predicted with acceptable accuracy from the sea surface elevation spectrum using linear theory, enabling comparisons to be made between the predicted and observed third-order statistics. The results indicate reasonable agreement between the predicted and observed vertical profiles of the vertical velocity skewness and asymmetry.

[49] Other effects of bottom slope and bottom friction on the vertical structure of the velocity field are as follows.

[50] 1. Bottom slope affects the magnitude of the vertical velocity only in the lower half of the water column, whereas the phase of vertical velocity relative to horizontal velocity and surface elevation is altered throughout the water column (Figures 2 and 5).

[51] 2. The departure from the horizontal bottom theory decreases with wave frequency, and increases as the bed is approached (Figures 4 and 5).

[52] 3. The measured and predicted vertical profiles of the third-order vertical velocity statistics, skewness and asym-

metry, exhibit pronounced differences from the profiles predicted for a horizontal bed. These strong depth dependence differences are governed by the changing relationships with depth among the skewness and asymmetry of the vertical and horizontal velocity components: that is, near the surface, $A_w \approx S_u$ and $S_w \approx -A_u$ since u and w are nearly in quadrature, whereas near the bottom, $A_w = A_u$ and $S_w = S_u$ since immediately above the WBL, u and w are forced by the bottom boundary condition to be in phase (Figures 9–12).

[53] Finally, because the vertical and horizontal velocities are not in quadrature in the presence of a sloping bed, a nonzero mean wave shear stress results which increases in magnitude toward the bed.

Appendix A: *Chu and Mei*'s [1970] Solutions for Stokes Waves Propagating Over a Sloping Sea Bed

[54] The following are the analytical solutions by *Chu and Mei* [1970]. Readers should refer to their paper for the detailed derivation. At $O(\varepsilon)$: for $n = 1$, $m = 0$, the boundary value problem is given by

$$R^{(1,0)} = F^{(1,0)} = G^{(1,0)} = H^{(1,0)} = 0 \tag{A1}$$

and the corresponding solutions are

$$\phi_z^{(1,0)} = 0 \tag{A2a}$$

$$\eta^{(1,0)} = 0. \tag{A2b}$$

For $n = 1$, $m = 1$, the solutions are

$$\phi^{(1,1)} = -\frac{ig}{\omega} A^{(1,1)} \cosh Q, \tag{A3a}$$

$$\eta^{(1,1)} = A^{(1,1)} \cosh q = \frac{1}{2} a, \tag{A3b}$$

where

$$Q = k(z+h), \quad q = k_0 h,$$

$$k \tanh kh = k_\infty = \frac{\omega^2}{g}.$$

At $O(\varepsilon^2)$:, for $n = 2$, $m = 0$, the boundary value problem is

$$R^{(2,0)} = F^{(2,0)} = G^{(2,0)} = 0 \tag{A4}$$

$$H^{(2,0)} = \frac{1}{4} g k_\infty a^2 \left(\sigma^2 - 1\right) + \phi_t^{(1,0)}, \tag{A5}$$

and the corresponding solution is

$$\eta^{(2,0)} = -\frac{1}{4} k_\infty a^2 \left(\sigma^2 - 1\right) - \frac{1}{g} \phi_t^{(1,0)}. \tag{A6}$$

For $n = 2$, $m = 1$, the boundary value problem is

$$R^{(2,1)} = -2i\vec{k} \cdot \nabla \phi^{(1,1)} - i\left(\nabla \cdot \vec{k}\right) \phi^{(1,1)}, \tag{A7a}$$

$$F^{(2,1)} = -\nabla h \cdot \left\{ i\vec{k} \phi^{(1,1)} \right\}_{z=-h}, \tag{A7b}$$

$$G^{(2,1)} = \left\{ i\left(\omega \phi^{(1,1)}\right)_t + i\omega \phi_t^{(1,1)} \right\}_{z=0}, \tag{A7c}$$

and the corresponding solutions are

$$H^{(2,1)} = \left\{ \phi_t^{(1,1)} \right\}_{z=0}, \tag{A8}$$

$$\frac{\phi^{(2,1)}}{\phi^{(1,1)}} = i\delta(X,Z), \tag{A9}$$

where

$$\delta(X,Z) = -\left[\alpha_1 (Q-q) + \alpha_2 (Q \tanh Q - q \tanh q) + \alpha_3 \left(Q^2 - q^2\right)\right], \tag{A10}$$

$$\alpha_1 = \frac{\vec{k}}{k} \cdot \nabla h, \tag{A11a}$$

$$\alpha_2 = \frac{\nabla \cdot \left[\frac{\vec{k}}{k} \left(A^{(1,1)}/\omega\right)^2\right]}{2k \left(A^{(1,1)}/\omega\right)^2}, \tag{A11b}$$

$$\alpha_3 = \frac{\vec{k} \cdot \nabla k}{2k^3}, \tag{A11c}$$

α_2 and α_3 are determined by the wave shoaling equation,

$$\vec{\nabla} \cdot \left(\vec{C}_g \frac{E}{\omega}\right) = 0 \tag{A12a}$$

where

$$C_g = \frac{1}{2} \frac{\omega}{k} \left(1 + \frac{2q}{\sinh 2q}\right) \tag{A12b}$$

$$E = \frac{1}{2} g a^2, \tag{A12c}$$

and the dispersion relationship

$$\omega^2 = gk \tanh kh. \tag{A13}$$

[55] **Acknowledgments.** We thank Bob Guza for helpful discussions of bottom slope effects, and Carolyn Smyth and Len Zedel for the preliminary processing of the CDP data. We also thank the anonymous reviewers for their constructive criticism. This research was supported by the Coastal Sciences Program of the U.S. Office of Naval Research and the Natural Science and Engineering Research Council of Canada.

References

Armstrong, J. A., N. Bloembergen, J. Ducuing, and P. S. Pershan, The interactions between light waves in a nonlinear dielectric, *Phys. Rev.*, *127*, 1918–1939, 1962.

Bendat, J. S., and A. G. Piersol, *Random Data: Analysis and Measurements Procedures*, 566 pp., Wiley-Interscience, New York, 1986.

Bretherton, F. P., Resonant interactions between waves: The case of discrete oscillations, *J. Fluid Mech.*, *20*, 457–480, 1964.

Bryant, P. J., Periodic waves in shallow water, *J. Fluid Mech.*, *59*, 625–644, 1973.

Chu, V. H., and C. C. Mei, On slowly varying Stokes waves, *J. Fluid. Mech.*, *41*, 873–887, 1970.

Crawford, A. M., and A. E. Hay, A simple system for laser-illuminated video imaging of sediment suspension and bed topography, *IEEE J. Oceanic. Eng.*, *23*, 12–19, 1999.

Crawford, A. M., and A. E. Hay, Linear transition ripple migration and wave orbital velocity skewness: Observations, *J. Geophys. Res.*, *106*, 14,113–14,128, 2001.

De Vriend, H. J., and N. Kitou, Incorporation of wave effects in a 3D hydrostatic mean current model, *Delft Hydraul. Rep. H-1295*, Delft, Netherlands, 1990.

Doering, J. C., and A. J. Bowen, Skewness in the nearshore zone, a comparison of estimates from Marsh-Mcbirney current meters and co-located pressure sensors, *J. Geophys. Res.*, *92*, 13,173–13,183, 1987.

Drennan, W. M., K. K. Kahma, and M. A. Donelan, The velocity field beneath wind-wave-observations and inferences, *Coastal Eng.*, *18*, 111–136, 1992.

Elgar, S., and R. T. Guza, Shoaling gravity waves, comparisons between field observations, linear theory, and a nonlinear model, *J. Fluid Mech.*, *158*, 47–70, 1985.

Elgar, S., M. H. Freilich, and R. T. Guza, Model-data comparisons of moments of nonbreaking shoaling surface gravity waves, *J. Geophys. Res.*, *95*, 16,055–16,063, 1990.

Elgar, S., B. Raubenheimer, and R. T. Guza, Current meter performance in the surf zone, *J. Atmos. Oceanic Technol.*, *18*, 1735–1746, 2001.

Freilich, M. H., and R. T. Guza, Nonlinear effects on shoaling surface gravity waves, *Philos. Trans. R. Soc. London, Ser. A*, *311*, 1–41, 1984.

Guza, R. T., and E. B. Thornton, Local and shoaled comparisons of sea surface elevations, pressures, and velocities, *J. Geophys. Res.*, *85*, 1524–1530, 1980.

Hasselmann, K., On the nonlinear energy transfer in a gravity wave spectrum part 1. General theory, *J. Fluid Mech.*, *12*, 481–500, 1962.

Herbers, T. H. C., R. L. Lowe, and R. T. Guza, Field observations of orbital velocities and pressure in weakly nonlinear surface gravity waves, *J. Fluid Mech.*, *245*, 413–435, 1992.

Liu, P. L.-F., S. B. Yoon, and J. T. Kirby, Nonlinear refraction-diffraction of waves in shallow water, *J. Fluid Mech.*, *153*, 185–201, 1985.

Mei, C. C., *The Applied Dynamics of Ocean Surface Waves*, 740 pp., Wiley-Interscience, New York, 1989.

Mei, C. C., and U. Unluata, Harmonic generation in shallow water waves, in *Waves on Beaches*, edited by R. E. Meyer, pp. 181–202, Academic, San Diego, Calf., 1972.

Phillips, O. M., On the dynamics of unsteady gravity waves of finite amplitude. part 1. The elementary interactions, *J. Fluid Mech.*, *9*, 193–217, 1960.

Rivero, F. J., and A. S. Arcilla, On the vertical-distribution of $\langle \tilde{u}\,\tilde{w} \rangle$, *Coastal Eng.*, *25*, 137–152, 1995.

Smyth, C., A. E. Hay, and L. Zedel, Coherent Doppler Profiler Measurements of Near-bed Suspended Sediment Fluxes and the Influence of Bedforms, *J. Geophys. Res.*, *107*(C8), 3105, doi:10.1029/2000JC000760, 2002.

Zedel, L., and A. E. Hay, A coherent Doppler profiler for high resolution particle velocimetry in the ocean: Laboratory measurements of turbulence and particle flux, *J. Atmos. Oceanic Technol.*, *16*, 1102–1117, 1999.

Zedel, L., and A. E. Hay, A three component bistatic coherent Doppler velocity profiler: Error sensitivity and system accuracy, *IEEE J. Oceanic Eng.*, *27*, 717–725, 2002.

Zou, Q.-P., An analytical model of wave bottom boundary layers incorporating turbulent relaxation and diffusion effects, *J. Phys. Oceanogr.*, *32*, 2441–2456, 2002.

Zou, Q.-P., and A. E. Hay, Velocity profiles above and within the wave bottom boundary layer over a sloping bottom, paper presented at ASCE 27th International Coastal Engineering Conference, Am. Soc. of Civ. Eng., Sydney, Australia, 2001.

Zou, Q.-P., and A. E. Hay, The vertical structure of the wave bottom boundary layer over a sloping bed: Theory and field measurements, *J. Phys. Oceanogr.*, *33*, 1380–1400, 2003.

A. J. Bowen, A. E. Hay, and Q. Zou, Department of Oceanography, Dalhousie University, Halifax, Nova Scotia, Canada B3H 4J1. (qingping@phys.ocean.dal.ca)